SGN – Assignment #2

Gabriele Nuccio, 247457

Exercise 1: Uncertainty propagation

You are asked to analyze the state uncertainty evolution along a transfer trajectory in the Planar Bicircular Restricted Four-Body Problem, obtained as optimal solution of the problem stated in Section 3.1 (Topputo, 2013)*. The mean initial state $\mathbf{x}_i$ at initial time t_i with its associated covariance $\mathbf{P}_0$ and final time t_f for this optimal transfer are provided in Table 1.

1. Propagate the initial mean and covariance within a time grid of 5 equally spaced elements going from t_i to t_f, using both a Linearized Approach (LinCov) and the Unscented Transform (UT). We suggest to use $\alpha = 1$ and $\beta = 2$ for tuning the UT in this case. Plot the mean and the ellipses associated with the position elements of the covariances obtained with the two methods at the final time.

2. Perform the same uncertainty propagation process on the same time grid using a Monte Carlo (MC) simulation †. Compute the sample mean and sample covariance and compare them with the estimates obtained at Point 1). Provide the following outputs.

   - Plot of the propagated samples of the MC simulation, together with the mean and the covariance obtained with all methods in terms of ellipses associated with the position elements at the final time.
   - Plot of the time evolution (for the time grid previously defined) for all three approaches (MC, LinCov, and UT) of $3\sqrt{\max(\lambda_i(P_r))}$ and $3\sqrt{\max(\lambda_i(P_v))}$, where P_r and P_v are the 2x2 position and velocity covariance submatrices.
   - Plot resulting from the use of the MATLAB function `qqplot`, for each component of the previously generated MC samples at the final time.

   Compare the results, in terms of accuracy and precision, and discuss on the validity of the linear and Gaussian assumption for uncertainty propagation.

Table 1: Solution for an Earth-Moon transfer in the rotating frame.

Parameter	Value
Initial state $\mathbf{x}_i$	$\mathbf{r}_i$ = [-0.011965533749906, -0.017025663128129]
	$\mathbf{v}_i$ = [10.718855256727338, 0.116502348513671]
Initial time t_i	1.282800225339865
Final time t_f	9.595124551366348
Covariance $\mathbf{P}_0$	$\begin{bmatrix} +1.041e-15 & +6.026e-17 & +5.647e-16 & +4.577e-15 \\ +6.026e-17 & +4.287e-18 & +4.312e-17 & +1.855e-16 \\ +5.647e-16 & +4.312e-17 & +4.432e-16 & +1.455e-15 \\ +4.577e-15 & +1.855e-16 & +1.455e-15 & +2.822e-14 \end{bmatrix}$

*F. Topputo, "On optimal two-impulse Earth–Moon transfers in a four-body model", Celestial Mechanics and Dynamical Astronomy, Vol. 117, pp. 279–313, 2013, DOI: 10.1007/s10569-013-9513-8.

†Use at least 1000 samples drawn from the initial covariance

1. To propagate the uncertainties, the initial mean state and covariance were propagated along the transfer trajectory using two methods: Linearized Covariance (LinCov) and Unscented Transform (UT). The results will be finally compared by analyzing the mean trajectory and the covariance ellipses at the final time.

   LinCov : In the LinCov method, the representation of the perturbed trajectory is considered sufficiently accurate under the assumption of linear dynamics. The mean state $\mathbf{x_0}$ and the covariance $\mathbf{P}_0$ are propagated using numerical integration of the linear dynamics equations of the Planar Bicircular Restricted Four-Body Problem (PBR4BP). The State Transition Matrix (STM), denoted as $\mathbf{\Phi}(t_0, t_i)$ is computed at each time step through variational approach. The propagated state and covariance are computed as:

   $$\hat{\mathbf{x}}_{LinCov}(t_i) = \varphi(\mathbf{x}_0, t_0, t_i), \quad \mathbf{P}_{LinCov}(t_i) = \mathbf{\Phi}(t_0, t_i)\mathbf{P}_0\mathbf{\Phi}(t_0, t_i)^T$$

   Therefore, the method aim to propagate the covariance of the state through the dynamics by using a first-order linearization, providing a good approximation for orbital motion in not-high non linear systems.

   UT : The Unscented Transform (UT) method is then adopted to propagate the initial state vector $\mathbf{x}_0$ and its corresponding covariance matrix $\mathbf{P}_0$ over time. In this method, assuming a Gaussian distribution, a set of sigma points ($\boldsymbol{\chi}_i$) were generated around the initial mean to parametrize the initial Probability Density Function (PDF) and then propagated through a nonlinear dynamics of the Planar Bicircular Restricted Four-Body Problem (PBR4BP) at each time step t_i. Finally, the mean and covariance are computed using weighted averages of the propagated sigma points $\boldsymbol{\gamma} = \boldsymbol{\varphi}(\boldsymbol{\chi_i}, t_0, t_i)$:

   $$\hat{\mathbf{x}}_{UT}(t_i) = \sum_{i=0}^{2n} W_i \gamma_i, \quad \mathbf{P}_{UT}(t_i) = \sum_{i=0}^{2n} W_i \left(\boldsymbol{\gamma}_i - \hat{\mathbf{x}}_{UT}(t_i)\right)\left(\boldsymbol{\gamma}_i - \hat{\mathbf{x}}_{UT}(t_i)\right)^T$$

   where W_i are the different weights.

The following plot shows the comparison of the two methods in terms of Mean Positions and Covariance Ellipses associated to the position elements.

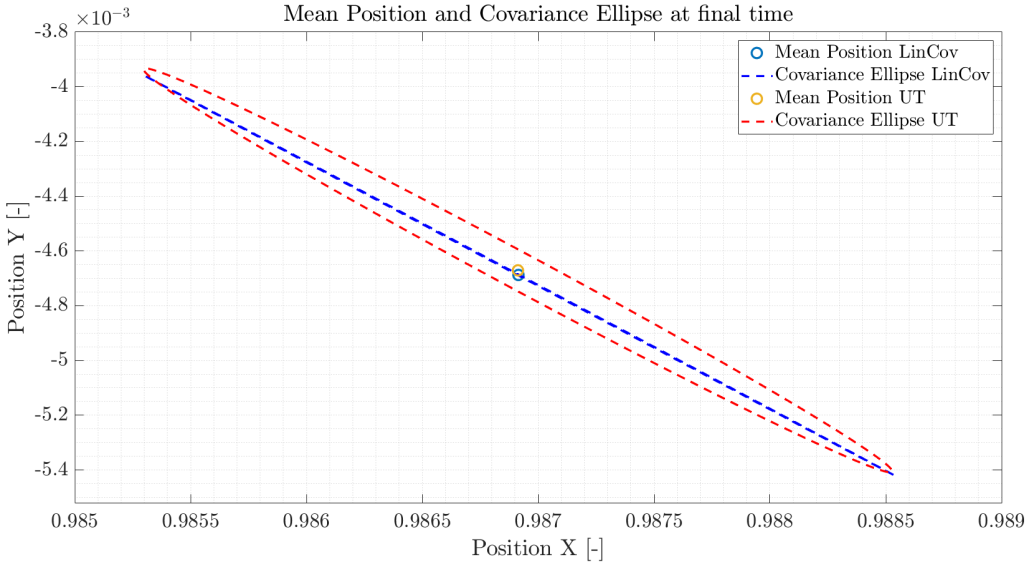

Figure 1: Comparison between LinCov and UT approaches in Earth-Moon Rotating Frame

The final mean and the final covariance are estimated better with the UT method with respect to the linear approximation. The differences between the results obtained by LinCov and UT are due to the initial assumptions. LinCov assumes that the uncertainty distribution remains Gaussian during propagation, and is based on a linearized dynamics around the mean state. On the other hand, UT assumes normality only for the initial distribution, and then the initial samples are propagated using the nonlinear dynamics model. Despite that, the mean state approximated with the linearized approach is close to the one estimated with the UT. This can be due to the fact that the dynamics presents a low non-linearity and to the limited propagation time. The distorted covariance ellipse of the LinCov method may result from the linear approximation of the dynamics, which does not fully capture the system's non-linearities. Moreover, LinCov may underestimate the distribution of uncertainties, in particular along the secondary directions of the trajectory, while in the primary direction it provides a comparable distribution.

2. To further develop the problem, a Monte Carlo (MC) simulation is performed to propagate the same initial uncertainty.

   Monte Carlo : the Monte Carlo approach is based on generating n samples from the mean state $\hat{\mathbf{x}}_0$ and the covariance matrix $\mathbf{P}_0$ assuming a multivariate gaussian random distribution generated with the function `mvnrnd` of `MatLab`. This distribution takes into account correlations between variables. Due to the high computational time embedded in a high number of samples, 1000 samples are selected as the minimum required by the problem. The samples are then mapped using the non-linear dynamics and finally the mean state and the covariance are computed from the propagated samples as follows:

$$\overline{\mathbf{x}}_{MC}(t_i) = \frac{1}{n}\sum_{i=1}^{n}\mathbf{y}_i(t_i), \quad \mathbf{P}_{MC}(t_i) = \frac{1}{n-1}\sum_{i=1}^{n}\left(\mathbf{y}_i(t_i) - \overline{\mathbf{x}}_{MC}(t_i)\right)\left(\mathbf{y}_i(t_i) - \overline{\mathbf{x}}_{MC}(t_i)\right)^T$$

   where $\mathbf{y}_i$ are the propagated MC samples.

The following plot shows the comparison of the three methods in terms of Mean Positions and Covariance Ellipses associated to the position elements. Furthermore the propagated Monte Carlo samples are also reported.

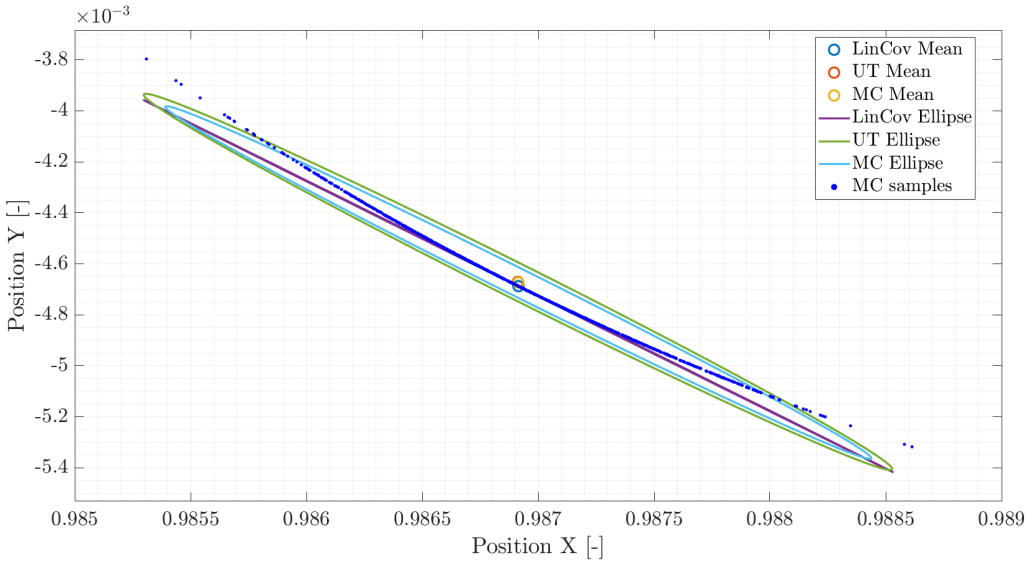

Figure 2: Comparison between LinCov, UT and MC approaches in Earth-Moon Rotating Frame

As shown in Fig. 2 The linear approximation method tends to underestimate the uncertainty around the mean, as evidenced by the smaller covariance ellipse compared to those derived from the MC and the UT approaches. Consistent with theoretical predictions, the mean and covariance obtained via the UT exhibit significantly better agreement with the results of the MC simulation. This highlights the superior capability of the UT in accurately capturing the system's nonlinear dynamics. As revealed in the plot, the MC samples fail in representing a Gaussian distribution, in fact some of them fall out of the covariance ellipse. However, the distribution is close to a normal one and thus validate the assumptions behind both LinCov and UT under the given conditions. Furthermore, using a higher number of samples for the MC simulation will lead to a enhanced similarity with the UT results in terms of mean state and covariance ellipse. On the other side this would require higher computational costs.

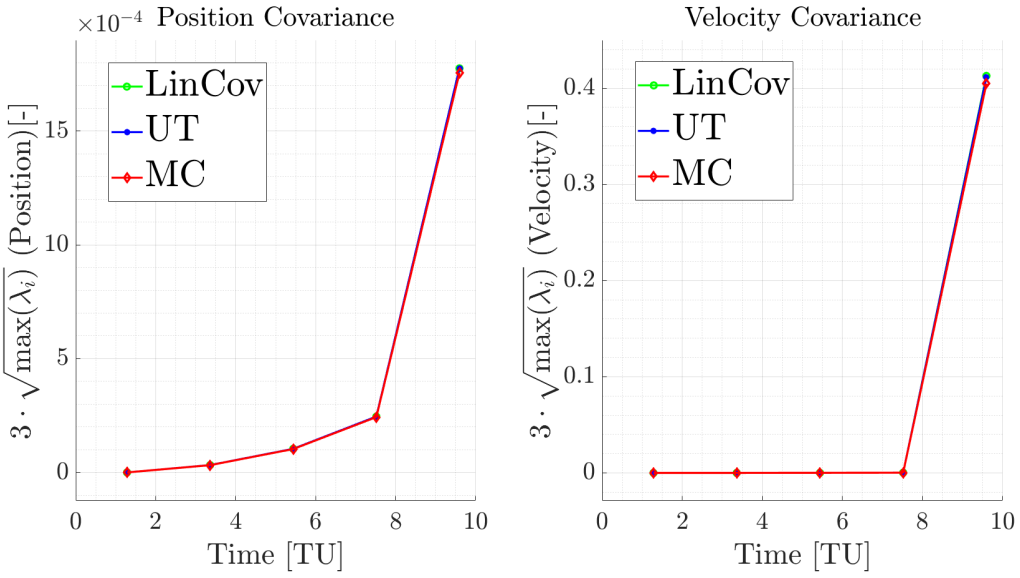

Figure 3: Evolution of the maximum square root of the eigenvalues of both position and velocity over time, computed with LinCov, UT and Monte Carlo

The previous observations are supported by the Fig. 3. This plot shows an increase of the maximum eigenvalues of both the position and velocity covariances. Moreover, MC and UT results in the maximum in standard deviations ($3\sigma_{max}$) exhibit their consistent convergence. At later time instants the LinCov method starts to deviate from the UT and MC trend, highlighting the limitations of the first-order linearisation. Furthermore, propagating for more time will increase the differences in terms of standard deviation between the linear approach and the UT and MC methods.

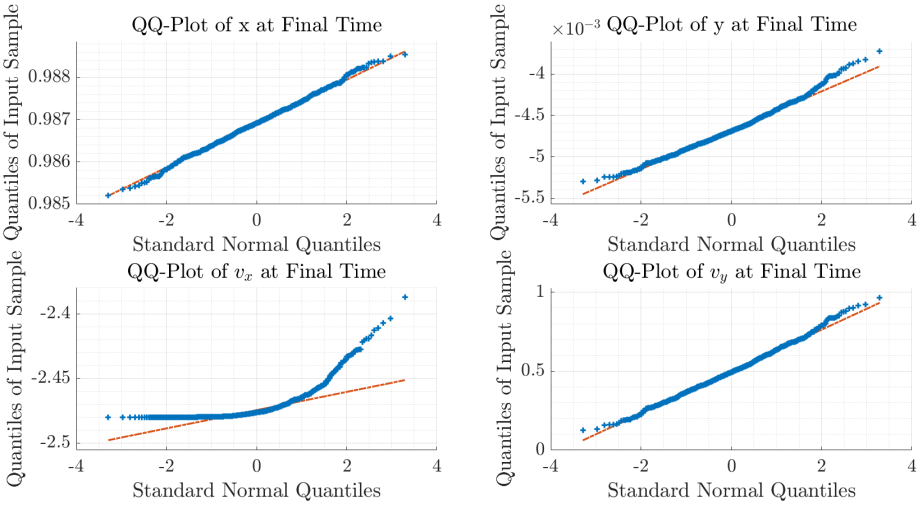

Figure 4: Q-Q plots for each state component of the propagated MC samples at the final time.

The Fig. 4 compare the theoretical quantiles of a normal distribution with the sample data quantiles in order to assess the normality of the distribution; from that the assumption of Gaussianity can be validated. The state components closely approximate a Gaussian distribution, as evidenced by the alignment of points along the reference line in the QQ-plots. Only the velocity component (v_x in particular), show more evident deviations reflecting the influence of the non-linear dynamics. This observation validates the Gaussianity assumption underlying both the LinCov and UT methods. However, it is important to note that this assumption may fall in the presence of highly nonlinear systems or for longer propagation times, where deviations from Gaussian behavior become more pronounced.
In conclusion, MC method provides the most accurate results but requires higher computational cost for an high number of samples. The LinCov method is definitely the least expensive computationally but lacks in reliability with non-linear dynamics performing well only in the primary direction of trajectory. Finally, the UT approach is the optimal one in terms of efficiency and accuracy robustness with uncertainty propagation problems.

Exercise 2: Batch filters

The Soil Moisture and Ocean Salinity (SMOS) mission, launched on 2 November 2009, is one of the European Space Agency's Earth Explorer missions, which form the science and research element of the Living Planet Programme.

You have been asked to track SMOS to improve the accuracy of its state estimate. To this aim, you shall schedule the observations from the three ground stations reported in Table 2.

1. *Compute visibility windows.* The Two-Line Elements (TLE) set of SMOS are reported in Table 3 (and in WeBeep as 36036.3le). Compute the osculating state from the TLE at the reference epoch t_{ref}, then propagate this state assuming Keplerian motion to predict the trajectory of the satellite and compute all the visibility time windows from the available stations in the time interval from $t_0 =$ `2024-11-18T20:30:00.000` (UTC) to $t_f =$ `2024-11-18T22:15:00.000` (UTC). Consider the different time grid for each station depending on the frequency of measurement acquisition. Report the resulting visibility windows and plot the predicted Azimuth and Elevation profiles within these time intervals.

2. *Simulate measurements.* Use SGP4 and the provided TLE to simulate the measurements acquired by the sensor network in Table 2 by:

   (a) Computing the spacecraft position over the visibility windows identified in Point 1 and deriving the associated expected measurements.

   (b) Simulating the measurements by adding a random error to the expected measurements (assume a Gaussian model to generate the random error, with noise provided in Table 2). Discard any measurements (i.e., after applying the noise) that does not fulfill the visibility condition for the considered station.

3. *Solve the navigation problem.* Using the measurements simulated at the previous point:

   (a) Find the least squares (minimum variance) solution to the navigation problem without a priori information using
   - the epoch t_0 as reference epoch;
   - the reference state as the state derived from the TLE set in Table 3 at the reference epoch;
   - the simulated measurements obtained for the KOROU ground station only;
   - pure Keplerian motion to model the spacecraft dynamics.

   (b) Repeat step 3a by using all simulated measurements from the three ground stations.

   (c) Repeat step 3b by using a J2-perturbed motion to model the spacecraft dynamics.

   Provide the results in terms of navigation solution[‡], square root of the trace of the estimated covariance submatrix of the position elements, square root of the trace of the estimated covariance submatrix of the velocity elements. Finally, considering a linear mapping of the estimated covariance from Cartesian state to Keplerian elements, provide the standard deviation associated to the semimajor axis, and the standard deviation associated to the inclination. Elaborate on the results, comparing the different solutions.

4. *Trade-off analysis.* For specific mission requirements, you are constrained to get a navigation solution within the time interval reported in Point 1. Since the allocation of antenna time has a cost, you are asked to select the passes relying on a budget of 70.000 €. The cost per pass of each ground station is reported in Table 2. Considering this constraint,

[‡]Not just estimated state or covariance

and by using a J2-perturbed motion for your estimation operations, select the best combination of ground stations and passes to track SMOS in terms of resulting standard deviation on semimajor axis and inclination, and elaborate on the results.

5. *Long-term analysis.* Consider a nominal operations scenario (i.e., you are not constrained to provide a navigation solution within a limited amount of time). In this context, or for long-term planning in general, you could still acquire measurements from multiple locations but you are tasked to select a set of prime and backup ground stations. For planning purposes, it is important to have regular passes as this simplifies passes scheduling activities. Considering the need to have *reliable* orbit determination and *repeatable* passes, discuss your choices and compare them with the results of Point 4.

Table 2: Sensor network to track SMOS: list of stations, including their features.

Station name	KOUROU	TROLL	SVALBARD
Coordinates	LAT = 5.25144° LON = -52.80466° ALT = -14.67 m	LAT = -72.011977° LON = 2.536103° ALT = 1298 m	LAT = 78.229772° LON = 15.407786° ALT = 458 m
Type	Radar (monostatic)	Radar (monostatic)	Radar (monostatic)
Measurements type	Az, El [deg] Range (one-way) [km]	Az, El [deg] Range (one-way) [km]	Az, El [deg] Range (one-way) [km]
Measurements noise (diagonal noise matrix R)	$\sigma_{Az,El}$ = 125 mdeg σ_{range} = 0.01 km	$\sigma_{Az,El}$ = 125 mdeg σ_{range} = 0.01 km	$\sigma_{Az,El}$ = 125 mdeg σ_{range} = 0.01 km
Minimum elevation	6 deg	0 deg	8 deg
Measurement frequency	60 s	30 s	60 s
Cost per pass	30.000 €	35.000 €	35.000 €

Table 3: TLE of SMOS.

```
1 36036U 09059A   24323.76060260  .00000600  00000-0  20543-3 0  9995
2 36036  98.4396 148.4689 0001262  95.1025 265.0307 14.39727995790658
```

1. The visibility windows of the SMOS satellite with respect to the three ground stations were computed using the Two-Line Elements (TLE) set provided in Table 3. First, the reference epoch date related to the given TLE was found: $t_{ref} = 2024-11-18\text{T}18:15:16.06464$. From the provided TLE and the reference epoch for SMOS satellite, the initial state at t_{ref} in ECI is retrieved rotating it from the TEME framework.

Position [x, y, z] [km]	[-6065.41379, 3768.04689, 14.50093]
Velocity $[v_x, v_y, v_z]$ [km/s]	[0.60362, 0.92674, 7.39077]

Table 4: SMOS osculating state

Then, using Keplerian dynamics the satellite position in the ECI reference frame at t_0. The propagator refers to the unperturbed 2 Body Problem dynamics.
The satellite's trajectory was thus propagated from t_0 to t_f considering the different time grids of each ground station. In fact, this is due to the different measurement frequencies provided in Table 2. The ground stations' state was expressed in the ECI reference frame and given with the `cspice_spkezr` function. After computing the relative state between SMOS and the ground stations, this was rotated in the Topocentric reference frame of each ground station. Finally, the `cspice_xmfsta` function provide the range, azimuth and elevation measurements.
After that, each visibility window associated to each ground station was determined by considering only the intervals when the SMOS satellite elevation is higher than the minimum detectable elevation by each of the GS provided in Table 2. In Table 5 the resulted windows within the given time interval are reported.

Station	Start Time (UTC)	End Time (UTC)	Total Duration (min)
Kourou	2024-11-18T20:40:00.000	2024-11-18T20:49:00.000	9
Troll	2024-11-18T21:02:30.000	2024-11-18T21:11:30.000	9
Svalbard	2024-11-18T21:56:00.000	2024-11-18T22:06:00.000	10

Table 5: Visibility windows for SMOS

Moreover, for each ground station the Azimuth and Elevation over time are reported on the left while on the right is exhibited the SMOS trajectory in terms of azimuth and elevation.

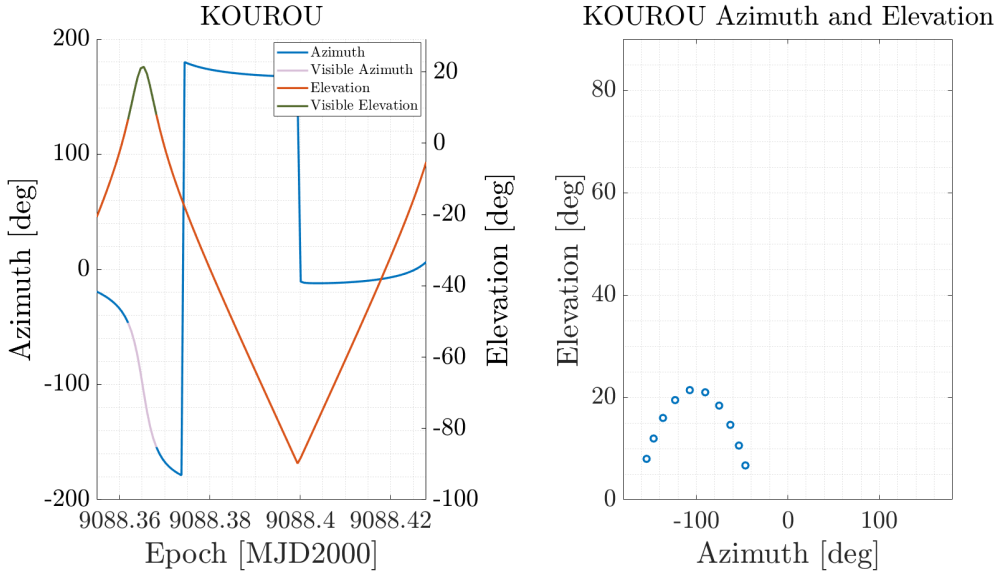

Figure 5: KOUROU station

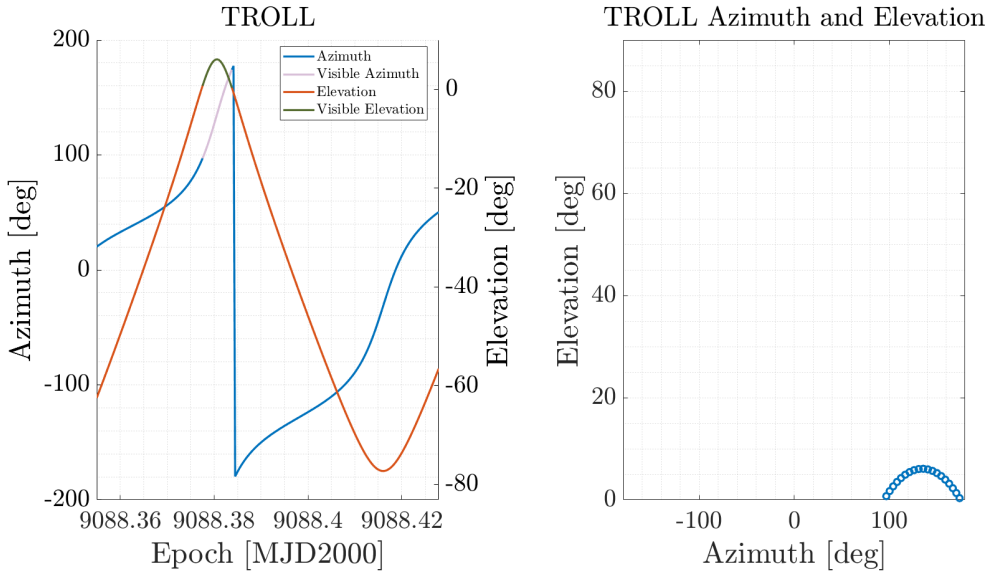

Figure 6: TROLL station

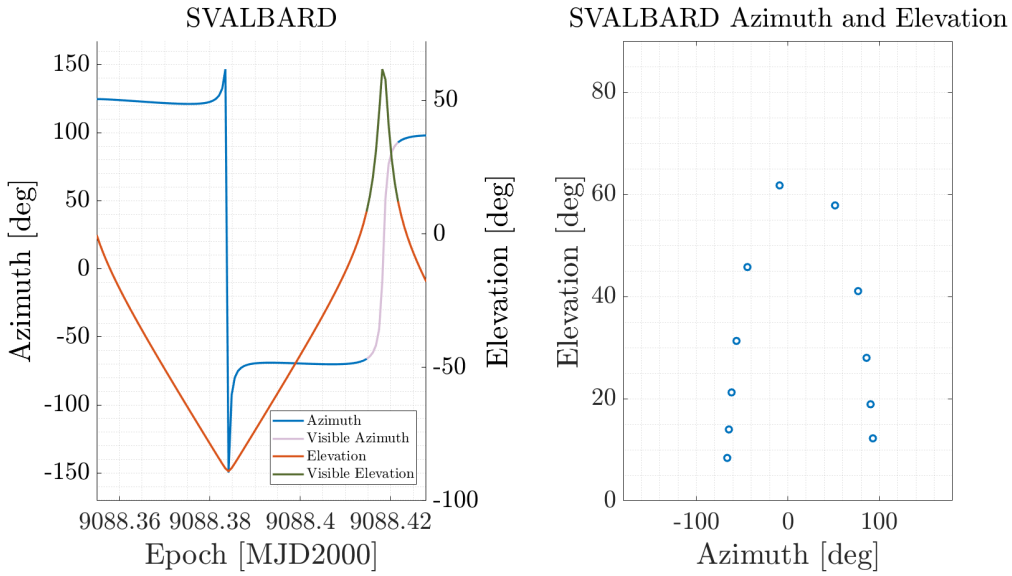

Figure 7: SVALBARD station

The plots display the periods where the SMOS satellite is visible, namely where the Elevation is higher than the minimum elevation associated with each of the GS. Moreover, the satellite's path in terms of Elevation and Azimuth is exhibited in the right plots. As can be seen, it starts with low elevation, it reaches a peak and then it starts descending back towards the horizon.

2. The second point of the exercise follows the same approach used in the first point, but this time adopting the SGP4 propagator. This takes into account the major perturbations: J2 effect, atmospheric drag, and the third-body perturbations. Some differences from the Keplerian propagator can be noted since the initial conditions are now provided directly from the TLE set. The satellite's trajectory is represented in a more accurate way by SGP4 and this can be seen in the Fig. 8

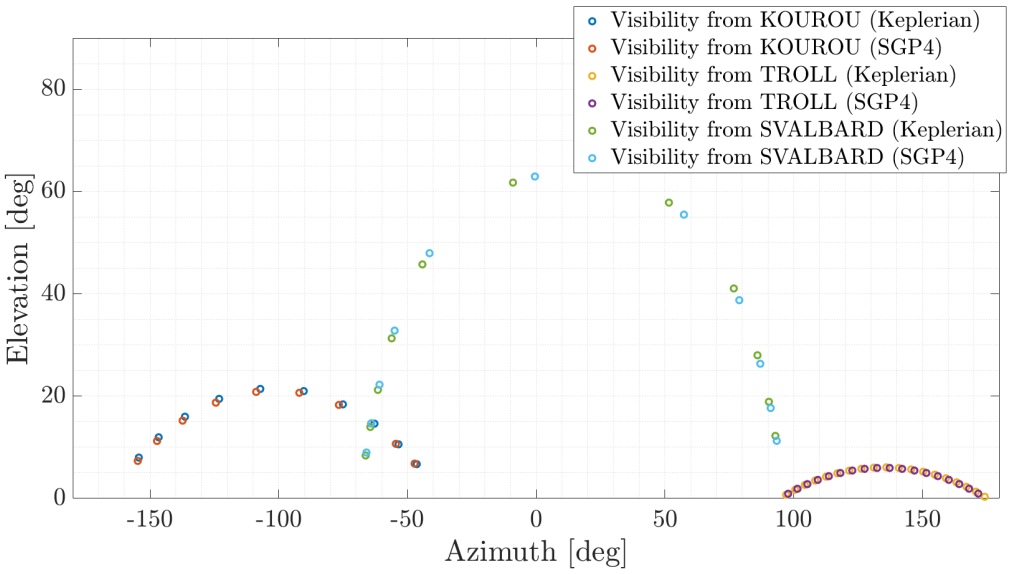

Figure 8: Comparison of visibility windows computed using the Keplerian propagator and SGP4

Afterwards, the simulated measurements (range, azimuth, elevation) were generated perturbing the ideal values with noises in Table 2, assuming a multivariate Gaussian distribution by using the `mvnrnd` function. The noise introduces additional deviations and thus makes measurements similar to real-world ones. After that, all the measurements not comprised in the visibility time windows are definitely discarded.

3. At this point a solution to the navigation problem is found under three different configurations: (a) using only measurements from Kourou GS, (b) using measurements from all the three GS and (c) incorporating the J_2-perturbed motion model. Furthermore, the Levenberg-Marquardt algorithm was selected for the non-linear least squares optimisation performed with `lsqnonlin` function. This algorithm is, in fact, better suited for cases where the initial guess may be relatively far from the optimal solution.

(a) Kourou Measurements Only

The workflow is performed as follows:

- Predicted measurements were computed with the same approach adopted in Ex 2.1
- The navigation problem was solved using a non linear least-squares optimization:

$$\min_{\mathbf{x_0}} \sum_{i=1}^{N} \mathbf{W}\mathbf{r}_i^T$$

where $\mathbf{r}_i$ are the residuals between predicted and observed measurements, and $\mathbf{W}$ is the weighting matrix computed from the respective measurements noises.

Position in ECI[x, y, z] [km]	[3938.13780, -1412.01134, 5778.50593]
Velocity in ECI[v_x, v_y, v_z] [km/s]	[4.87655, -3.76667, -4.23872]
$\sqrt{tr(\mathbf{P}_{rr})}$[km]	6.828836
$\sqrt{tr(\mathbf{P}_{vv})}$[km/s]	0.008400
Standard deviation of semi-major axis [km]	6.706492
Standard deviation of inclination [deg]	0.0493393

Table 6: Navigation Solution at time t_0 in ECI using Kourou only

$$\mathbf{P_0} = \begin{bmatrix} 38.115356 & 3.951197 & -1.520527 & -0.040793 & -0.013983 & -0.020213 \\ 3.951197 & 4.689349 & -4.101708 & -0.002686 & -0.003412 & 0.004048 \\ -1.520527 & -4.101708 & 3.828293 & 0.000244 & 0.002081 & -0.004986 \\ -0.040793 & -0.002686 & 0.000244 & 0.000044 & 0.000014 & 0.000024 \\ -0.013983 & -0.003412 & 0.002081 & 0.000014 & 0.000007 & 0.000005 \\ -0.020213 & 0.004048 & -0.004986 & 0.000024 & 0.000005 & 0.000020 \end{bmatrix}$$

Table 7: Covariance Matrix at time t_0 in ECI using Kourou only. Units: $[km^2], [km^2/s], [km^2/s^2]$

The output presented in Table 6 and Table 7 include the Navigation solution in Cartesian coordinates, the covariance matrix and the square root of the trace of the covariance submatrices for both position and velocity and the standard deviations for the semi-major axis and inclination, computed via linear mapping of the estimated covariance from Cartesian state to Keplerian elements. Here, the procedure underlying the linear mapping is reported. In order to estimate the Jacobian matrix to transform the Cartesian state $(\mathbf{r}, \mathbf{v})$ into Keplerian elements $(a, e, i, \Omega, \omega, \theta)$, the forward finite differences were used. To assess this, a perturbation ε for each component of the state is introduced. The computation of this latter comes from the floating-point relative accuracy (`eps`) in `MatLab` and computed as:

$$\varepsilon_i = \sqrt{\texttt{eps}} \cdot \max(1, |x_i|)$$

where x_i are the components of the state.
The Jacobian is then computed as:

$$\mathbf{J} = \begin{bmatrix} \frac{\partial \varphi}{\partial \mathbf{x}_0} & \frac{\partial \varphi}{\partial \mathbf{y}_0} & \frac{\partial \varphi}{\partial \mathbf{z}_0} & \frac{\partial \varphi}{\partial \mathbf{v}_{x0}} & \frac{\partial \varphi}{\partial \mathbf{v}_{y0}} & \frac{\partial \varphi}{\partial \mathbf{v}_{z0}} \end{bmatrix}$$

where with forward differentiation for each component of the state:

$$\frac{\partial \varphi}{\partial x_i} = \frac{\varphi(\mathbf{x}_0 + \boldsymbol{\varepsilon}_i, t_0, t) - \varphi(\mathbf{x}_0, t_0, t)}{\varepsilon_i}$$

Afterwards, the estimated covariance matrix of the Keplerian elements is computed from the Jacobian and the covariance matrix of the Cartesian state as $\mathbf{P_{kep}} = \mathbf{J}\mathbf{P_{car}}\mathbf{J}$. Finally, the estimated standard deviation for the semi-major axis and the inclination are the square root of the first and third components on the diagonal of the estimated covariance matrix respectively. This linear approximation is valid under the assumption of small uncertainties in Cartesian state. It provides an efficient way to evaluate the impact of the uncertainties on orbit parameters. Finally, $\sqrt{tr(\mathbf{P}_{rr})}$ and $\sqrt{tr(\mathbf{P}_{vv})}$ -respectively the trace of the position and velocity covariance submatrices- give a measurement of the uncertainty in the initial state estimate.

(b) All Ground Stations Measurements

In this configuration, all the three GS measurements were used in order to improve the estimation accuracy. The predicted measurements are now computed for each ground station within the visibility time window reported in Ex 2.1. It is worth of notice that the same Keplerian propagator was adopted to model the SMOS' trajectory. Combining the different ground stations contributes the measurements are further improved. Again, a

least-squares optimization was performed, now considering all the stations data combined. The optimization function is:

$$\min_{\mathbf{x_0}} \sum_{j=1}^{3} \sum_{i=1}^{N} \mathbf{W}_j \mathbf{r}_{i,j}^T$$

where $\mathbf{r}_{i,j}$ are the residuals between predicted and observed i-th measurement at the j-th station, and $\mathbf{W}$ is the weighting matrix computed from the respective measurements noises for that station j.

Position in ECI[x, y, z] [km]	[3926.94995, -1411.08353, 5780.00881]
Velocity in ECI[v_x, v_y, v_z] [km/s]	[4.88849, -3.76497, -4.23341]
$\sqrt{tr(\mathbf{P}_{rr})}$[km]	1.105012
$\sqrt{tr(\mathbf{P}_{vv})}$[km/s]	0.001144
Standard deviation of semi-major axis [km]	0.132567
Standard deviation of inclination [deg]	0.002018

Table 8: Navigation Solution at time t_0 in ECI using all the GS

$$\mathbf{P_0} = \begin{bmatrix} 0.714997 & -0.443276 & -0.146740 & -0.000724 & 0.000239 & -0.000476 \\ -0.443276 & 0.410583 & 0.127711 & 0.000500 & -0.000128 & 0.000347 \\ -0.146740 & 0.127711 & 0.095471 & 0.000118 & -0.000042 & 0.000139 \\ -0.000724 & 0.000500 & 0.000118 & 8.187782e-7 & -2.063179e-7 & 4.882220e-7 \\ 0.000239 & -0.000128 & -0.000042 & -2.063179e-7 & 1.245158e-7 & -1.537103e-7 \\ -0.000476 & 0.000347 & 0.000139 & 4.882220e-7 & -1.537103e-7 & 3.646697e-7 \end{bmatrix}$$

Table 9: Covariance Matrix at time t_0 in ECI using all the GS. Units: $[km^2], [km^2/s], [km^2/s^2]$

The results reported include the navigation solution combining data from all the stations. As noticed, increasing the number of measurements decrease the uncertainty on the outputs. This is clearly displayed with the reduced Covariance values and the improved standard deviations.

(c) J_2-Perturbed Motion

As final request, also the J_2 perturbation is modeled to take into account the effect of the Earth's oblateness. Now the Keplerian dynamics comprise also acceleration of the J_2 perturbation resulting in a total acceleration computed as:

$$\ddot{\mathbf{r}} = -\mu \frac{\mathbf{r}}{|\mathbf{r}|^3} + \mathbf{a}_{J_2}$$

This is, as before, numerically integrated. Furthermore, the same procedure for the least-squares optimization combining the three stations measurements is followed.

Position in ECI[x, y, z] [km]	[3932.75059, -1414.91246, 5778.50315]
Velocity in ECI[v_x, v_y, v_z] [km/s]	[4.87981, -3.76322, -4.23287]
$\sqrt{tr(\mathbf{P}_{rr})}$[km]	0.025937
$\sqrt{tr(\mathbf{P}_{vv})}$[km/s]	2.688891e-05
Standard deviation of semi-major axis [km]	0.003399
Standard deviation of inclination [deg]	5.021601e-05

Table 10: Navigation Solution at time t_0 in ECI using all the GS and applying J_2-perturbed dynamics

$$\mathbf{P_0} = \begin{bmatrix} 4.0938\text{e-}04 & -2.3715\text{e-}04 & -4.3731\text{e-}05 & -4.1978\text{e-}07 & 1.4178\text{e-}07 & -2.3159\text{e-}07 \\ -2.3715\text{e-}04 & 2.1973\text{e-}04 & 3.6516\text{e-}05 & 2.7888\text{e-}07 & -6.8007\text{e-}08 & 1.4954\text{e-}07 \\ -4.3731\text{e-}05 & 3.6516\text{e-}05 & 4.3611\text{e-}05 & 1.8965\text{e-}08 & -1.2832\text{e-}08 & 4.5412\text{e-}08 \\ -4.1978\text{e-}07 & 2.7888\text{e-}07 & 1.8965\text{e-}08 & 4.9057\text{e-}10 & -1.2076\text{e-}10 & 2.3541\text{e-}10 \\ 1.4178\text{e-}07 & -6.8007\text{e-}08 & -1.2832\text{e-}08 & -1.2076\text{e-}10 & 7.9065\text{e-}11 & -7.9337\text{e-}11 \\ -2.3159\text{e-}07 & 1.4954\text{e-}07 & 4.5412\text{e-}08 & 2.3541\text{e-}10 & -7.9337\text{e-}11 & 1.5338\text{e-}10 \end{bmatrix}$$

Table 11: Covariance Matrix at time t_0 in ECI using all the GS and applying J_2-perturbed dynamics. Units: $[km^2], [km^2/s], [km^2/s^2]$

The outputs here comprise the refined navigation solution, further reduced covariance values for position and velocity, and further improved standard deviations for the semi-major axis and inclination.
The results clearly illustrate how variations in ground station configurations and dynamic models influence the accuracy of the navigation solutions. Relying solely on a single ground station, such as Kourou, significantly increases uncertainties in position and velocity estimation due to limited visibility and a constrained observation time window. This is evident from the covariance matrix analysis, which reveals substantially larger errors when observations are restricted to the Kourou station only. Incrementally incorporating data from additional ground stations, such as Troll and Svalbard, and subsequently including J_2 perturbations in the dynamic model, yields a marked improvement in the accuracy of position and velocity estimations for the SMOS satellite. Table 8 and Table 10 quantitatively demonstrate this enhancement. The integration of observations from multiple ground stations effectively extends the cumulative observation time window by combining the tracking intervals of individual stations, thereby providing more comprehensive coverage of the satellite's trajectory. Furthermore, incorporating the J_2-perturbed dynamic model enhances the fidelity of the satellite's predicted trajectory by accounting for perturbative effects induced by Earth's oblateness. This refinement reduces residuals between predicted measurements and simulated observations (as computed in Exercise 2.2b), further improving the solution's accuracy. Examining the standard deviations of the semi-major axis and inclination obtained through linear mapping reveals a progressive reduction in their magnitude, consistent with the decrement of the covariance matrix elements. This trend reflects an improvement in the precision of the observations, driven by the refinement of the dynamic model and by the increasing of the available measurements.

4. As required by the maximum mission budget and after verifying that only one passage per each ground station occurs within the time window in point 2.1, the maximum number of ground station to be used to select the best combination is two. As explained in Ex 2.3 (c), the J_2 perturbed model is adopted but now only taking into account two of three available GS. Therefore three possible combinations of two GS can be selected.

GS	σ of semi-major axis [km]	σ of inclination [deg]
Kourou - Troll	1.051124	0.002189
Kourou - Svalbard	0.023294	6.419267e-04
Troll - Svalbard	0.046718	3.182569e-04

Table 12: Standard deviations of semi-major axis and inclination for three possible alternatives of the Trade-off analysis

The performance is primarily influenced by the geometric diversity of the network and the orbital coverage and visibility of the stations involved in the measurements. An ideal network would include stations positioned at significantly different latitudes to provide complementary measurements. Moreover, because of SMOS' polar orbit, stations at higher latitudes are more effective for estimating the orbit inclination, whereas stations in equatorial locations, such as Kourou, offer greater precision in determining the semi-major axis. As illustrated in Table 12, the second configuration achieves the highest accuracy in semi-major axis estimation, while the third configuration provides the best results for inclination accuracy. However, these outcomes represent just one possible scenario. Due to the stochastic nature of the noisy measurements, the results may vary with each iteration of the analysis. By iteratively performing the procedure and evaluating the positions of the ground stations on Earth, a definitive conclusion can be performed. The optimal configuration is the combination of the Kourou and Svalbard stations, which consistently yields the highest accuracy for the semi-major axis and, in enough cases, superior results for the inclination. This advantage arises because, within the given time window from t_0 to t_f, the satellite's trajectory passes directly over the Kourou station, making its measurements particularly beneficial. Furthermore, the complementary geographical positions of the Kourou station (at a low latitude) and the Svalbard station (at a high latitude) enhance the accuracy of the observations by providing diverse vantage points. On the other side, the combination Troll-Svalbard provides accurate estimates of the orbit inclination but performs worse for the semi-major axis, because both stations are located at high latitudes. The selected configuration not only improves measurement precision but also reduces operational costs, assessing the total expenditure to 65,000$.

5. To build on the last point of this exercise, the visibility windows were extended to simulate a real-world scenario where the time intervals are increased. To ensure higher accuracy, the initial state derived from the TLEs provided in Table 2 was propagated both forward and backward by five hours from the reference epoch. This five hours interval represents the maximum time span over which the TLEs are considered reliable. The following plots provide key insights into the impact of these extended time windows and allow for critical evaluation of their implications. Moreover, the results summarised in Table 13 show the total observation time available for each station.

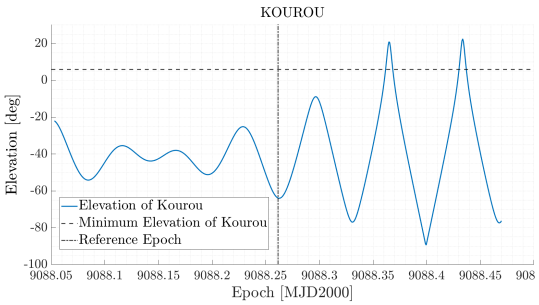

Figure 9: Elevation of Kourou

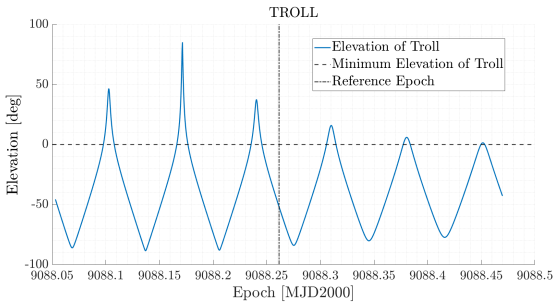

Figure 10: Elevation of Troll

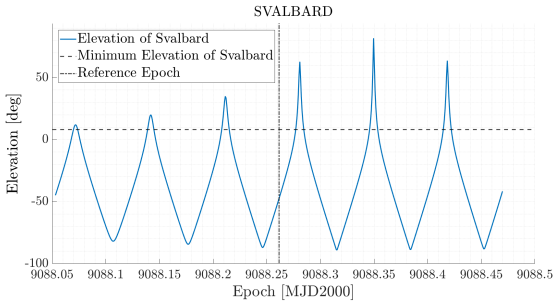

Figure 11: Elevation of Svalbard

Station	Total observation time [min]
Kourou	18
Troll	71
Svalbard	56

Table 13: Time windows for 12 hours

The table reveals that Troll and Svalbard ensure significantly more observation time compared to Kourou. This difference is due to Kourou's low-latitude location, which, despite being advantageous for accurate measurements during specific passes, does not allow for frequent and repeatable observations in a polar trajectory such the one given in this exercise. The satellite's orbit in fact, being polar, moves over different regions of the Earth over time, and Kourou's position near the equator limits the number of passes it can observe, especially in a long term analysis. In contrast, Troll and Svalbard, located at higher latitudes, respectively in the North and South hemispheres, benefit from their positioning relative to the satellite's orbit, enabling more repeatable passes due to the frequent coverage in polar regions that is where SMOS spends the majority of its trajectory. Repeatability is a critical factor for long-term operations, where the ability to schedule regular passes without significant gaps between them simplifies operational planning, and ensures precision in orbital paramters determination, in particular inclination. Given that repeatability is essential, Troll and Svalbard should be prioritized as the primary stations. Therefore, this is the most robust solution for orbit tracking. Kourou instead plays a backup role in the network of stations. As, in fact, the Point 4 results stand, Kourou station could be very helpful and preferable over the other stations in particular circumstances: such as when high precision is required for a short-term segment of the mission or in the event of a failure of one of the primary stations. Using Kourou station during SMOS equatorial passes will provide instead an higher accuracy in semi-major axis.

Exercise 3: Sequential filters

An increasing number of lunar exploration missions will take place in the next years, many of them aiming at reaching the Moon's surface with landers. In order to ensure efficient navigation performance for these future missions, space agencies have plans to deploy lunar constellations capable of providing positioning measurements for satellites orbiting around the Moon.

Considering a lander on the surface of the Moon, you have been asked to improve the accuracy of the estimate of its latitude and longitude (considering a fixed zero altitude). To perform such operation you can rely on the use of a lunar orbiter, which uses its Inter-Satellite Link (ISL) to acquire range measurements with the lander while orbiting around the Moon. At the same time, assuming the availability of a Lunar Navigation Service, you are also receiving measurements of the lunar orbiter inertial position vector components, such that you can also estimate the spacecraft state within the same state estimation process.
To perform the requested tasks you can refer to the following points.

1. *Check the visibility window.* Considering the initial state $\mathbf{x}_0$ and the time interval with a time-step of 30 seconds from t_0 to t_f reported in Table 14, predict the trajectory of the satellite in an inertial Moon-centered reference frame assuming Keplerian motion. Use the estimated coordinates given in Table 15 to predict the state of the lunar lander. Finally, check that the lander and the orbiter are in relative visibility for the entire time interval.

2. *Simulate measurements.* Always assuming Keplerian motion to model the lunar orbiter dynamics around the Moon, compute the time evolution of its position vector in an inertial Moon-centered reference frame and the time evolution of the relative range between the satellite and the lunar lander. Finally, simulate the measurements by adding a random error to the spacecraft position vector and to the relative range. Assume a Gaussian model to generate the random error, with noise provided in Table 14 for both the relative range and the components of the position vector. Verify (graphically) that the applied noise level is within the desired boundary.

3. *Estimate the lunar orbiter absolute state.* As a first step, you are asked to develop a sequential filter to narrow down the uncertainty on the knowledge of the lunar orbiter absolute state vector. To this aim, you can exploit the measurements of the components of its position vector computed at the previous point. Using an Unscented Kalman Filter (UKF), provide an estimate of the spacecraft state (in terms of mean and covariance) by sequentially processing the acquired measurements in chronological order. To initialize the filter in terms of initial covariance, you can refer to the first six elements of the initial covariance $\mathbf{P}_0$ reported in Table 14. For the initial state, you can perturb the actual initial state $\mathbf{x}_0$ by exploiting the MATLAB function `mvnrnd` and the previously mentioned initial covariance. We suggest to use $\alpha = 0.01$ and $\beta = 2$ for tuning the UT in this case. Plot the time evolution of the error estimate together with the 3σ of the estimated covariance for both position and velocity.

4. *Estimate the lunar lander coordinates.* To fulfill the goal of your mission, you are asked to develop a sequential filter to narrow down the uncertainty on the knowledge of the lunar lander coordinates (considering a fixed zero altitude). To this aim, you can exploit the measurements of the components of the lunar orbiter position vector together with the measurements of the relative range between the orbiter and the lander computed at the previous point. Using an UKF, provide an estimate of the spacecraft state and the lunar lander coordinates (in terms of mean and covariance) by sequentially processing the acquired measurements in chronological order. To initialize the filter in terms of initial covariance, you can refer to the initial covariance $\mathbf{P}_0$ reported in Table 14. For the initial state, you can perturb the actual initial state, composed by $\mathbf{x}_0$ and the latitude

and longitude given in Table 15, by exploiting the MATLAB function `mvnrnd` and the previously mentioned initial covariance. We suggest to use $\alpha = 0.01$ and $\beta = 2$ for tuning the UT in this case. Plot the time evolution of the error estimate together with the 3σ of the estimated covariance for both position and velocity.

Table 14: Initial conditions for the lunar orbiter.

Parameter	Value
Initial state $\mathbf{x}_0$ [km, km/s]	$\mathbf{r}_0$ = [4307.844185282820, -1317.980749248651, 2109.210101634011] $\mathbf{v}_0$ = [-0.110997301537882, -0.509392750828585, 0.815198807994189]
Initial time t_0 [UTC]	2024-11-18T16:30:00.000
Final time t_f [UTC]	2024-11-18T20:30:00.000
Measurements noise	σ_p = 100 m
Covariance $\mathbf{P}_0$ [km^2, km^2/s^2, rad^2]	`diag([10,1,1,0.001,0.001,0.001,0.00001,0.00001])`

Table 15: Lunar lander - initial guess coordinates and horizon mask

Lander name	MOONLANDER
Coordinates	LAT = 78° LON = 15° ALT = 0 m
Minimum elevation	0 deg

1. Given the initial state $\mathbf{x_0}$ the trajectory of the satellite is propagated from initial time t_0 to the final time t_f using Keplerian dynamics the satellite's position in the Inertial Moon-Centred (MCI) reference frame. The propagator refers to the unperturbed 2 Body Problem dynamics.

   Afterwards, from the initial guess coordinates of the lander in Table 15, the initial state can be computed. The position vector comes from the `cspice_latrec` function of `MatLab`, while the velocity is a zero vector in the Moon Centred Moon Fixed (MCMF) frame since the lander is assumed to rotate with the same lunar velocity. After that, a rotation is computed with the `cspice_sxform` function to transform the lander state from MCMF into MCI reference frame. The lander state is presented in Table 16:

x [km]	y [km]	z [km]	v_x [km/s]	v_y [km/s]	v_z [km/s]
348.917	93.492	1699.434	0	0	0

Table 16: Lunar Lander Initial State in MCMF at t_0

   Finally, the relative position of the satellite with the lander is estimated and the elevation can be derived to check the visibility windows. As Fig. 13 exhibits during the entire time interval, the relative visibility between the orbiter and the lander is ensured as demonstrated by the Elevation profile, this latter is, in fact, always over the minimum of 0°.

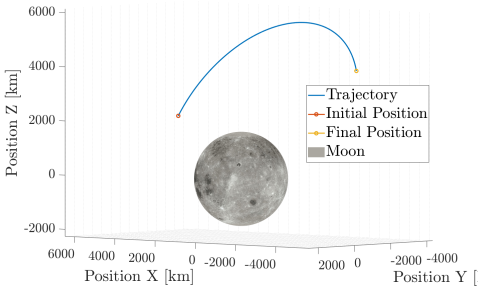

Figure 12: Orbiter Trajectory around Moon (@Moon MCI frame)

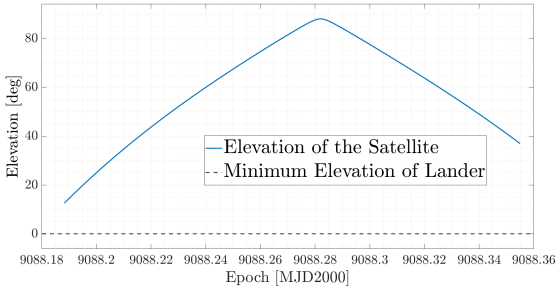

Figure 13: Elevation

2. In this point both the evolution of the Lunar Orbiter's position vector and of the relative range with respect to Lunar Lander are evaluated. This time, to estimate the position of the lander, the provided kernels are adopted by using the function `cspice_spkezr`. By following the same procedure of Exercise 3.1 the relative range is finally computed.

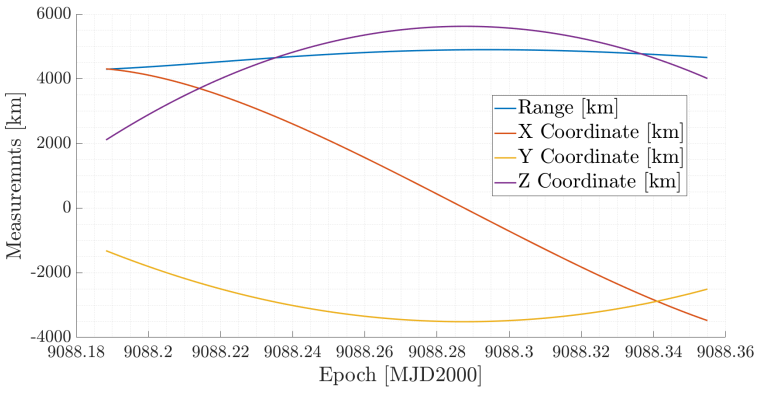

Figure 14: Position and Range over time in MCI

Furthermore, a random error is applied to both position and range from the noise provided in Table 14. Plotting the relative error between the ideal measurements and the real ones with the $\pm 3\sigma$ value, the hypothesis of Gaussianity can be confirmed.

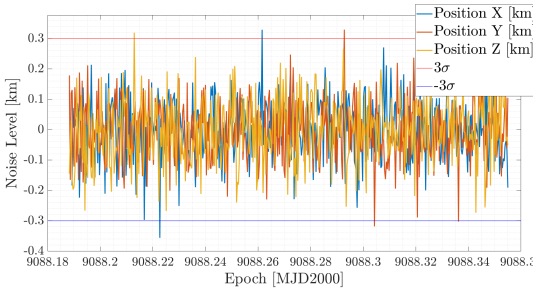

Figure 15: Noise Level of Position

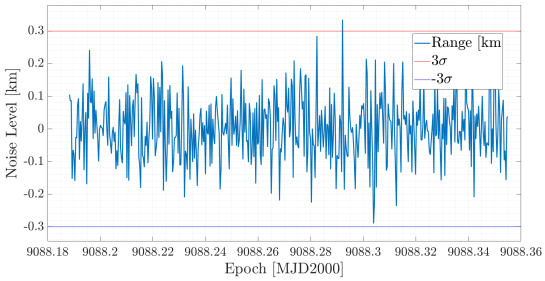

Figure 16: Noise Level of Range

As showcased in Fig. 15 and Fig. 16, the assumption of normality for the noise distribution is validated. Specifically, over 99% of the noise values for both position and range fall within the expected bounds of $\pm 3\sigma$, confirming the statistical behavior consistent with a Gaussian distribution. This statement indicates that the noise model is robust and accurately represents inherent uncertainties.

3. In this point an Unscented Kalman Filter (UKF) is used to narrow down the uncertainty on the state vector of the lunar orbiter. This UKF exploit the sequentiality of the acquired measurements and the Unscented Transform (UT). A more in-depth description of the algorithm is showcased in Algorithm 1.

Position in (@Moon MCI) [x, y, z] [km]	[-3479.005045, -2506.17970 , 4010.73665]
Velocity in (@Moon MCI) $[v_x, v_y, v_z]$ [km/s]	[-0.45012, 0.34854, -0.55779]

Table 17: Final Mean State at time t_f

$$\mathbf{P_f} = \begin{bmatrix} 7.19023\text{e-}05 & 6.74014\text{e-}06 & -1.08017\text{e-}05 & 5.70695\text{e-}09 & 3.56510\text{e-}09 & -5.70538\text{e-}09 \\ 6.74014\text{e-}06 & 8.14872\text{e-}05 & -2.81973\text{e-}05 & 5.24611\text{e-}09 & 8.87056\text{e-}09 & -9.42292\text{e-}09 \\ -1.08017\text{e-}05 & -2.81973\text{e-}05 & 1.08929\text{e-}04 & -8.38634\text{e-}09 & -9.42097\text{e-}09 & 1.80491\text{e-}08 \\ 5.70695\text{e-}09 & 5.24611\text{e-}09 & -8.38634\text{e-}09 & 1.96596\text{e-}12 & 1.22052\text{e-}12 & -1.95130\text{e-}12 \\ 3.56510\text{e-}09 & 8.87056\text{e-}09 & -9.42097\text{e-}09 & 1.22052\text{e-}12 & 1.95720\text{e-}12 & -1.86908\text{e-}12 \\ -5.70538\text{e-}09 & -9.42292\text{e-}09 & 1.80491\text{e-}08 & -1.95130\text{e-}12 & -1.86908\text{e-}12 & 3.77770\text{e-}12 \end{bmatrix}$$

Table 18: Final Covariance Matrix at time t_f (@Moon MCI). Units: $[km^2], [km^2/s], [km^2/s^2]$

In Table 17 and Table 18 are presented the final mean state and the final covariance matrix exiting from the sequential filter.

Algorithm 1 `Unscented Kalman Filter (UKF)`

Input: Initial state $\mathbf{x}_0$, Initial covariance $\mathbf{P}_0$, Real measurements, Measurement noise covariance, UKF parameters α, β, λ
Output: Estimated state $\mathbf{x}_k^+$, Covariance $\mathbf{P}_k^+$
Compute Weights $W_i^{(m)}$, $W_i^{(c)}$ from UKF parameters
for each k from 1 to length(t_{Span}) - 1 **do**
Prediction Step:
Generate sigma points $\boldsymbol{\chi}_{i,k-1}$ from $\hat{\mathbf{x}}_{k-1}^+$ and $\mathbf{P}_{k-1}^+$
Propagate sigma points with 2 Body Problem non-linear dynamics: $\boldsymbol{\chi}_{i,k}$
Compute predicted state mean: $\hat{\mathbf{x}}_k^-$ using $W_i^{(m)}$
Compute predicted covariance: $\mathbf{P}_k^+$ using $W_i^{(c)}$
Measurement Update:
Transform sigma points to measurement space: $\boldsymbol{\gamma}_{i,k}$ applying the measurement function
Compute predicted measurement mean: $\hat{\mathbf{y}}_k^-$ using $W_i^{(m)}$
Compute the measurement covariance taking into account the measurement noise covariance: $\mathbf{P}_{ee,k}$
Compute cross-covariance: $\mathbf{P}_{xy,k}$
Compute Kalman gain: $\mathbf{K}_k$
Update state using Real Measurements: $\hat{\mathbf{x}}_k^+$
Update covariance: $\mathbf{P}_k^+$
end for

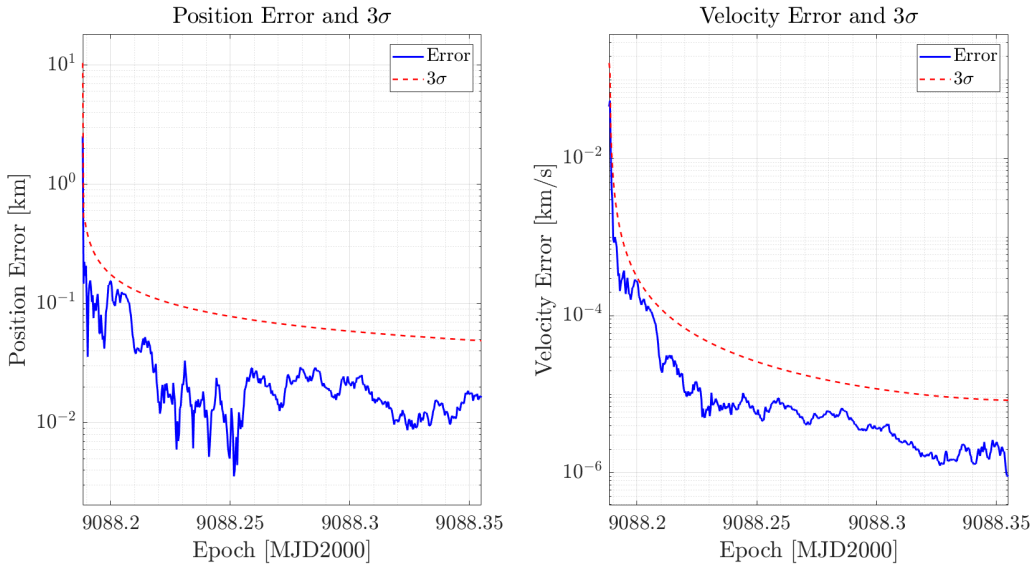

Figure 17: Position and Velocity Error over time

The plots exhibited in Fig. 17 represent the position error and velocity error behavior over time. These latter are computed between the reference trajectory and the state vector computed with the UKF. Initially, the errors are relatively high due to the perturbed initial state, but as the filter processes more measurements, both position and velocity errors and their corresponding standard deviations decrease over time, reflecting the expected correlation between them. The errors remain within the 3σ bound throughout the simulation time, validating the Gaussian assumption. Furthermore, the position error decreases less compared to the velocity error. This latter error shows, in fact, a faster convergence, due to the dominance of the deterministic orbital dynamics in velocity propagation.

4. The last point of the exercise follow the same rationale of Ex 3.3, but now introducing

another measurement namely the relative range between orbiter and lander. This latter is computed by converting the lander's coordinates to Cartesian coordinates in the Moon-Centered Inertial (MCI) frame and then performing the norm of the difference between the orbiter propagated sigma points and the transformed lander position. Moreover, the initial state is composed by $\mathbf{x}_0$ and the latitude and longitude of the moonlander and provided in Table 15. The complete initial covariance matrix is thus adopted.

Estimated state $\mathbf{x}_f$ [km, km/s, deg, deg]	$\mathbf{r}_f$ (@Moon MCI frame) = [-3479.00737, -2506.18017, 4010.73726] $\mathbf{v}_f$ (@Moon MCI frame) = [-0.45012, 0.34854, -0.55779] lat_f = 78.2247 lon_f = 15.3999

Table 19: Final estimated state and Lander coordinates at t_f for the Lunar Orbiter and Lander.

$$\mathbf{P_f} = \begin{bmatrix} 6.317\text{e-}05 & 4.291\text{e-}06 & -6.913\text{e-}06 & 3.772\text{e-}09 & 2.679\text{e-}09 & -4.287\text{e-}09 & -2.621\text{e-}07 & -2.716\text{e-}07 \\ 4.291\text{e-}06 & 8.174\text{e-}05 & -2.867\text{e-}05 & 5.174\text{e-}09 & 8.852\text{e-}09 & -9.399\text{e-}09 & -2.893\text{e-}07 & -2.573\text{e-}07 \\ -6.913\text{e-}06 & -2.867\text{e-}05 & 1.098\text{e-}04 & -8.306\text{e-}09 & -9.411\text{e-}09 & 1.804\text{e-}08 & 4.678\text{e-}07 & 4.142\text{e-}07 \\ 3.772\text{e-}09 & 5.174\text{e-}09 & -8.306\text{e-}09 & 1.773\text{e-}12 & 1.141\text{e-}12 & -1.826\text{e-}12 & -5.588\text{e-}11 & -6.267\text{e-}11 \\ 2.679\text{e-}09 & 8.852\text{e-}09 & -9.411\text{e-}09 & 1.141\text{e-}12 & 1.924\text{e-}12 & -1.818\text{e-}12 & -5.397\text{e-}11 & -4.611\text{e-}11 \\ -4.287\text{e-}09 & -9.399\text{e-}09 & 1.804\text{e-}08 & -1.826\text{e-}12 & -1.818\text{e-}12 & 3.698\text{e-}12 & 8.575\text{e-}11 & 7.275\text{e-}11 \\ -2.621\text{e-}07 & -2.893\text{e-}07 & 4.678\text{e-}07 & -5.588\text{e-}11 & -5.397\text{e-}11 & 8.575\text{e-}11 & 1.040\text{e-}08 & 1.146\text{e-}08 \\ -2.716\text{e-}07 & -2.573\text{e-}07 & 4.142\text{e-}07 & -6.267\text{e-}11 & -4.611\text{e-}11 & 7.275\text{e-}11 & 1.146\text{e-}08 & 1.360\text{e-}08 \end{bmatrix}$$

Table 20: Covariance matrix at time t_f (@Moon MCI frame). Units: $[km^2], [km^2/s], [km^2/s^2], [km\ rad], [km/s\ rad], [rad^2]$

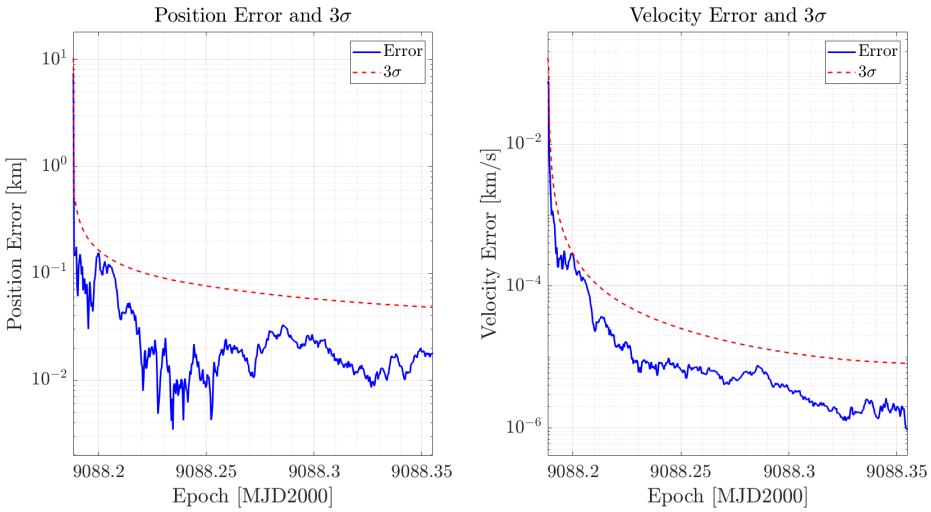

Figure 18: Position and Velocity Error over time

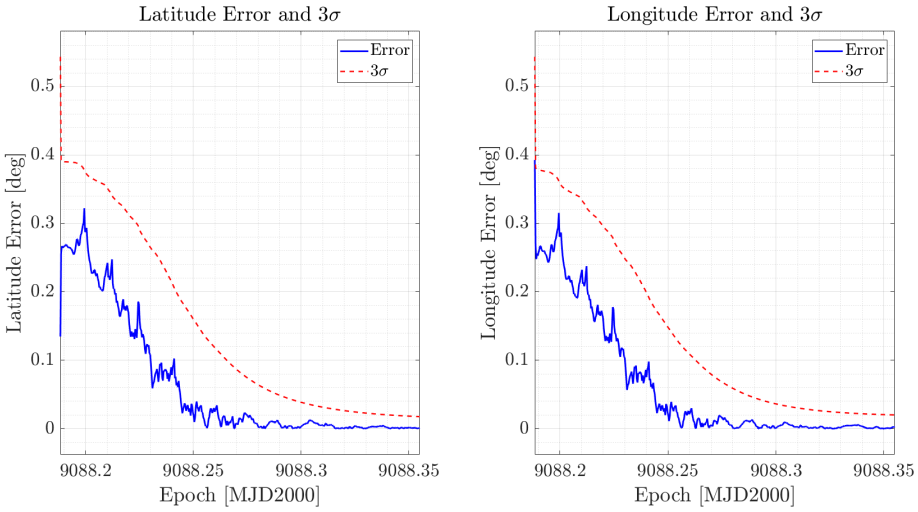

Figure 19: Latitude and Longitude Error over time

The plots exhibited in Fig. 18 represent the position error and velocity error behavior over time, while the ones presented in Fig. 19 the latitude and longitude errors. Again, as expected, both the errors and their corresponding standard deviations decrease over time. All errors here remain within the 3σ bound throughout the simulation time, validating the Gaussian assumption for all components of the state. Due to the stochastic nature of the analysis, this latter was performed multiple times to assess its validity. Moreover, in some cases, the latitude and longitude errors plotted in Fig. 19 can exceed their related standard deviations for short times. However, the estimated orbiter state remains within the bounds as expected. The non-linearities in the relationship between orbiter position and the relative range measurements could be the driving force of the coordinates error behaviour. This consideration highlights some limitations in the UKF model. However, the sequential filter is reliable but, some improvements on the accuracy of the noise level or in better approximating high order terms would be taken into account to achieve better performances.